Journal of Inflammation Research

Dovepress
Taylor & Francis Group

Open Access Full Text Article

ORIGINAL RESEARCH

Kadsua coccinea Extract Alleviates Rheumatoid Arthritis via TNF-α Suppression and Gut Microbiota Modulation

Hao Zheng[1,2,*], Jiaxin Yang[1,*], Yasi Deng[1], Bowen Zhang[1], Fan Bai[1], Yuxin Chen[1], Yunmi Lu[1], Beier Lian[1], Juan Huang[1], Yupei Yang[1], Wei Wang[1], Huanghe Yu[1]

[1]TCM and Ethnomedicine Innovation & Development International Laboratory, Innovative Materia Medica Research Institute, School of Pharmacy, Hunan University of Chinese Medicine, Changsha, 410208, People's Republic of China; [2]Hunan Provincial Key Laboratory of the Research and Development of Novel Pharmaceutical Preparations, School of Pharmacy, Changsha Medical University, Changsha, 410219, People's Republic of China

*These authors contributed equally to this work

Correspondence: Huanghe Yu; Wei Wang, TCM and Ethnomedicine Innovation & Development International Laboratory, Innovative Materia Medica Research Institute, School of Pharmacy, Hunan University of Chinese Medicine, Changsha, 410208, People's Republic of China, Email yhh@hnucm.edu.cn; wangwei402@hotmail.com

Background and Purpose: *Kadsura coccinea*, Lem. A. C. Smith (KCR) is a traditional multi-ethnic medicinal plant in China, widely used by Yao, Dong, and other ethnic groups in Hunan, Yunnan, Guangxi, and other southern regions. Traditionally prepared as medicinal wine, it has shown notable therapeutic advantages in treating rheumatoid arthritis (RA), though its underlying mechanism remains unclear.

Methods: This study evaluated the anti-RA effects of KCR ethanol extract in vitro and in vivo using LPS-induced RA fibroblast-like synoviocytes (RAFLS) and inflammatory macrophages (RAW264.7), as well as an adjuvant-induced arthritis (AIA) rat model generated with inactivated Mycobacterium tuberculosis. Mechanisms were explored via network pharmacology, molecular biology, and gut microbiota analysis.

Results: KCR extract suppressed TNF-α, IL-1β, and IL-6 expression in LPS-stimulated RAFLS and RAW264.7 cells. It markedly inhibited paw swelling, synovial hyperplasia, and bone destruction in AIA rats, potentially by downregulating TNF-α, IL-1β, and IL-6 in paw tissues and modulating gut microbiota (*Corynebacterium* and *Jeotgalicoccus*). At 3000 mg/kg, no significant histopathological or hematological toxicity was observed.

Conclusion: Collectively, KCR alleviates joint pathologies in AIA rats by suppressing TNF-α-driven inflammation and modulating gut microbiota, with *Corynebacterium* and *Jeotgalicoccus* identified as potential mediators of the TNF-α-gut axis. These findings underscore KCR's anti-RA efficacy and mechanisms, providing a theoretical basis for its safe clinical application and promoting further development.

Keywords: Yao ethnomedicine, *Kadsura coccinea* (Lem.) A. C. Smith, rheumatoid arthritis, inflammatory response, gut microbiota

Introduction

Rheumatoid arthritis (RA), an autoimmune inflammatory disease affecting approximately 1% of the global population, is characterized by chronic synovial inflammation leading to bone destruction, the main cause of disability.[1,2] Current first-line therapeutics for RA include glucocorticoids, non-steroidal anti-inflammatory drugs (NSAIDs), disease-modifying antirheumatic drugs (DMARDs), and immunosuppressants.[3] While these agents alleviate clinical symptoms and suppress disease progression, they frequently induce severe adverse effects including hepatotoxicity, nephrotoxicity, gastrointestinal hemorrhage, and osteoporosis.[4,5] Consequently, identifying novel safe and effective RA treatments remains imperative.

Kadsura coccinea, Lem. A. C. Smith (KCR), a root herb from the Schisandraceae family (Schisandra genus) and commonly called "Heilaohu" in Yao ethnomedicine, is a core component of traditional Yao medicinal formulations. Its traditional pharmacological actions include activating Qi, promoting blood circulation, dispelling wind-dampness,

https://doi.org/10.2147/JIR.S557108
Received: 30 July 2025
Accepted: 4 March 2026
Published: 7 April 2026

Graphical Abstract

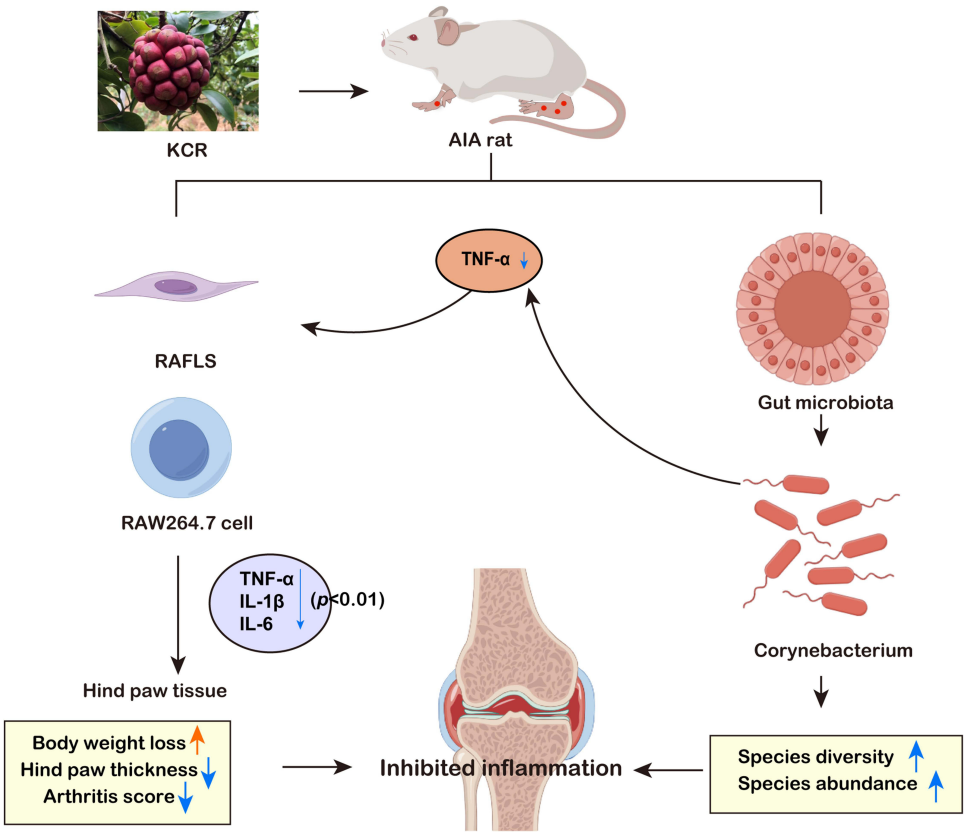

dredging meridians, resolving blood stasis, and alleviating pain. Clinically, it is primarily prescribed for RA and joint pain in Yao ethnic medicine.[6,7] A substantial number of triterpenoids, sesquiterpenoids, and lignans were isolated from KCR in our preliminary study. Among these, triterpenoids and sesquiterpenoids significantly inhibited the proliferation of RA fibroblast-like synoviocytes (RAFLS) in vitro, suggesting these compounds may constitute the primary active anti-RA components. However, the precise mechanism and therapeutic targets of KCR for RA treatment have not yet been elucidated.

In patients with RA, a complex interplay of pro-inflammatory factors drives synovial hyperplasia and bone destruction.[8–10] Macrophages and lymphocytes secrete key pro-inflammatory cytokines including tumor necrosis factor-α (TNF-α), interleukin-17 (IL-17), and interleukin-6 (IL-6), which activate the nuclear factor kappa-B (NF-κB) signaling pathway to initiate inflammatory cascades.[11] TNF-α stimulates rheumatoid arthritis fibroblast-like synoviocyte (RAFLS) proliferation and lymphocyte activity, while IL-17 and IL-6 synergistically recruit/activate neutrophils, monocytes, and other immune cells to form a self-perpetuating inflammatory feedback loop; together with interleukin-1β (IL-1β) and macrophage colony-stimulating factor (M-CSF), these cytokines disrupt joint microenvironment homeostasis by promoting abnormal synovial cell growth and drive B cell differentiation into plasma cells that produce anti-citrullinated protein antibodies (ACPA), rheumatoid factor (RF), and immune complexes, exacerbating autoimmune responses and synovial invasion. Notably, TNF-α plays a central role in the Th17 signaling pathway: dendritic cell-tissue cell interaction induces T cell differentiation into Th17 cells, triggering IL-17A/IL-17F release to sustain chronic inflammation.[12,13] This inflammatory cascade ultimately leads to the upregulation of matrix metalloproteinases, accelerating the degradation of the extracellular matrix and causing irreversible damage to articular cartilage and bone tissue.

Clinically, the levels of these inflammatory factors are significantly elevated in the joints of RA patients compared to healthy controls, underscoring their critical role in disease pathogenesis.[8]

Gut microbiome dysbiosis, characterized by an imbalance in the gut microbial community, has emerged as a significant factor in the development of various autoimmune diseases, including RA.[9] Direct clinical evidence has confirmed that gut microbiota dysbiosis precedes the onset of RA in susceptible individuals by 5–10 years, with specific microbial taxa (eg, *Segatella copri, Corynebacterium*) driving synovial inflammation and joint destruction via multiple pathways. For instance, dysregulated gut microbiota can enhance intestinal permeability ("leaky gut"), allowing microbial antigens to translocate into the circulation and trigger cross-reactive autoimmune responses against joint tissues via molecular mimicry,[10,11] and can also promote systemic secretion of TNF-α that directly mediate synovial hyperplasia and bone erosion in RA.[12] Among the diverse bacterial genera implicated, *Corynebacterium* has drawn particular research attention: its overabundance in RA patients is closely correlated with disease activity and joint damage severity, and it can initiate or exacerbate inflammatory processes by upregulating TNF-α production and disrupting immune tolerance.[13] Although the exact mechanisms linking Actinobacteria, to which *Corynebacterium* belongs, to RA remain unclear, this association highlights the potential role of gut microbiota dysbiosis and specific bacterial species in the pathogenesis of extra - intestinal inflammatory diseases. The metabolites produced by the gut microbiota play a crucial role in immune response modulation. Short - chain fatty acids (SCFAs), including butyrate, propionate, and acetate, are generated through the anaerobic fermentation of dietary fibers by gut bacteria. These SCFAs are involved in regulating the differentiation and function of immune cells. In dysbiotic states, the decreased production of SCFAs reduces their anti-inflammatory effects. Consequently, the suppression of pro-inflammatory T-cell activation is compromised, and the development of regulatory T cells (Tregs) is hindered. This immunological imbalance skews the immune response towards a pro-inflammatory state, promoting the release of cytokines such as TNF-α, IL-1β, and IL-6, which are key drivers of RA pathogenesis.[14] Another mechanism by which gut microbiota may contribute to RA is molecular mimicry. Bacterial antigens with structural similarities to host proteins can trigger the immune system to produce antibodies that cross react with self-antigens in joints. For example, it is hypothesized that certain epitopes on gut bacteria may share structural features with proteins in the synovial tissues of RA patients, thereby initiating an autoimmune cascade that leads to joint inflammation and destruction.[15] Considering TNF-α's role in both gut barrier dysfunction and microbial dysbiosis, we propose a hypothesis: KCR may regulate RA through a TNF-α-gut microbiota axis, integrating anti-inflammatory and microbiome modulating effects.

This study systematically explored KCR's therapeutic potential in RA via a multi-step approach: network pharmacology predicted potential targets, followed by molecular docking between KCR's main components and key targets to investigate molecular interactions. In vitro experiments used LPS-induced RAFLS/RAW264.7 cell models to assess anti-inflammatory effects, while in vivo AIA rat models mimicked RA pathology, with comprehensive analysis of gut microbiome composition, taxonomic differences, and marker species in intestinal contents. Additionally, KCR's oral safety was evaluated in mice by determining the maximum tolerated dose and assessing effects on major organs, providing insights into its therapeutic mechanism, supporting RA treatment development, and promoting rational application of ethnomedicine-based therapies.

Materials and Methods

Reagents

The KCR voucher specimen (2015071501) was preserved in the International Laboratory of Innovative Development of Traditional Chinese Medicine and Ethnomedicine, Institute of Innovative Materia Medica, School of Pharmacy, Hunan University of Chinese Medicine, Changsha, Hunan Province, China, after collecting KCR in Huaihua city, Hunan Province. Lipopolysaccharide (LPS), Triptolide, phenylmethylsulfonyl fluoride (PMSF), ethylenediaminetetraacetic acid (EDTA), dimethyl sulfoxide (DMSO), Fetal bovine serum (FBS) and Bovine type II collagen were purchased from Solarbio Co., Ltd (Beijing, China); Protein Phosphatase Inhibitor was purchased from SEVEN Co., Ltd (Beijing, China); Inactivated Mycobacterium tuberculosis H37Ra was purchased from BD Co., Ltd (NJ, USA); Liquid paraffin

were purchased from Sigma-Aldrich Co., Ltd (MO, USA); TNF-α antibody (AF7014), IL-6 antibody (DF6087), IL-1β antibody (AF5103), β-actin antibody (AF7018), and Goat Anti-Rabbit IgG (H+L) HRP antibody (S0001).

High Performance Liquid Chromatography (HPLC)-Diode Array Detector (DAD) Analysis of Isolated Compounds in KCR

A 5 μL aliquot of both the control solution and KCR test solution was precisely pipetted and injected into the HPLC system for chromatographic analysis. After detection, the similarity between the test sample's fingerprint and the reference chromatogram was calculated via full-spectrum peak matching, in compliance with the Traditional Chinese Medicine Chromatographic Fingerprint Similarity Evaluation System. To ensure the quality and consistency of the KCR extract, only samples with a similarity value ≥ 0.90 were deemed eligible for subsequent experiments.

Prediction of Drug Targets for KCR in RA

After isolation and purification of KCR, 42 compounds were obtained. Their SMILES structural formulas were generated using ChemDraw and Chem3D software. The SMILES sequences were then uploaded to the Swiss Target Prediction Database (http://swisstargetprediction.ch/) for target prediction.

Prediction of Targets for RA

RA-related targets were searched from the following databases: GeneCards database (https://www.genecards.org/), DisGeNET database (https://www.disgenet.org/home/), DrugBank database (https://go.drugbank.com/), OMIM database (https://www.omim.org/), and TTD database (http://db.idrblab.net/ttd/).

Construction of Protein-Protein Interaction (PPI) Network, Kyoto Encyclopedia of Genes and Genomes (KEGG) and Gene Ontology (GO) Enrichment Analyses

The STRING database (https://string-db.org/) was utilized to construct a PPI network of interacting targets between KCR and RA, with the genus set as Homo sapiens and a confidence score > 0.900. The Network Analyzer plugin for Cytoscape 3.9.0 was employed to analyze the topology of the PPI network. Core targets were identified by filtering based on centrality metrics (degree, closeness, and betweenness), with key targets selected using median information values of these metrics. KEGG and GO enrichment analyses were performed using the ClusterProfiler package in R 3.18.

Molecular Docking Analysis

Molecular docking simulations were performed using the AutoDock Vina 1.1.2 program. Two-dimensional and three-dimensional conformations of KCR compounds were prepared using ChemDraw and Chem3D 14.0, respectively. The 3D structure of TNF-α (PDB ID: 2AZ5) was retrieved from the RCSB Protein Data Bank. To identify potential binding sites, the DoGSiteScorer server (https://proteins.plus) was used to predict docking pockets on the TNF-α protein. One optimal pocket was selected as the docking site for subsequent analyses. Following docking, conformations with the lowest binding energy and highest docking scores were chosen as the most favorable binding modes for further characterization.[16,17]

Animals

A total of 36 male Sprague-Dawley (SD) rats (70–90 g, n=36) were purchased from Beijing Vital River Laboratory Animal Technology Co., Ltd. and housed in the specific pathogen-free (SPF) Experimental Animal Center of Hunan University of Chinese Medicine (permit number: 202302190001); for the AIA model experiment, rats were stratified into 6 groups (normal group n=6, model group n=6, triptolide group n=6, KCR 200/400/800 mg/kg groups n=6 per group). Additionally, 20 male and 20 female ICR mice (approximately 20 g, total n=40) were obtained from the same supplier and bred in the SPF facility of Hunan University of Chinese Medicine (permit number: HNUCM21-2501-20); for the safety evaluation experiment, mice were divided into 2 groups (control group n=20, KCR treatment group n=20, with equal numbers of male and female mice in each group).

Cell Culture

RAFLS and RAW264.7 cells were purchased from Procell Life Science & Technology Co., Ltd (Wuhan, China). RAFLS were cultured in DMEM/F-12 (1:1) medium supplemented with 10% FBS (Grand Island, USA) and 1% penicillin/streptomycin, while RAW264.7 cells were maintained in DMEM medium with the same supplements. Both cell types were incubated at 37°C under 5% CO_2.

Cell Treatment and Cytokine Detection

The ethanol extract of KCR was dissolved in DMSO, diluted to a concentration of 0.4 mg/mL and then filtered through a 0.22 μm membrane, followed by serial dilution to 0.2 mg/mL and 0.1 mg/mL, respectively. The concentrations of KCR (0.1–0.4 mg/mL) and triptolide (1.6 mg/mL) were selected based on preliminary dose-finding experiments.[7] RAFLS (2.5×10^5 cells/well) were seeded into 6-well plates and stimulated with LPS (400 ng/mL) for 6 h. The medium was then replaced with DMEM/F-12 (1:1) basic medium containing KCR (0.1/0.2/0.4 mg/kg) or TRI (1.6 mg/mL), followed by 24 h incubation. Cells were collected for Western blotting to detect TNF-α, IL-1β, IL-6, and β-actin expression. RAW264.7 cells (2.5×10^5 cells/well) were inoculated into 6-well plates, treated with LPS (400 ng/mL) for 6 h, and then cultured in DMEM basic medium supplemented with KCR (0.1/0.2/0.4 mg/kg) or TRI (1.6 mg/mL) for 24 h. Cell lysates were analyzed for the aforementioned cytokines and β-actin via Western blotting.

Western Blotting Analysis of Cellular Protein

KCR ethanol extract was dissolved in DMSO, filtered through a 0.22 μm membrane, and serially diluted to 0.1, 0.2, and 0.4 mg/mL. After KCR treatment (0.1–0.4 mg/mL), cells were harvested and lysed in pre-cooled RIPA buffer containing PMSF and phosphatase inhibitors. Lysates were ice-incubated for 45 min, centrifuged (12,000 rpm, 4°C, 20 min), and supernatants were collected for protein quantification via BCA assay.

Total proteins were separated by 6–12% SDS-PAGE gels (based on protein size), transferred to PVDF membranes, and blocked with 5% skim milk. Membranes were incubated overnight at 4°C with primary antibodies (TNF-α, IL-1β, IL-6, β-actin), washed, and probed with HRP-conjugated secondary antibodies for 2 h at room temperature. Protein bands were visualized using a Tanon fluorescence imager and quantified by Image J software.

AIA Model Establishment

Rats were acclimatized for 7 days prior to modeling. AIA was induced in 70–90 g male SD rats by subcutaneous injection of 200 μL complete Freund's adjuvant (CFA) emulsion containing 2 mg/mL heat-inactivated Mycobacterium tuberculosis at the tail base. After immunization, AIA rats (excluding the normal group) were randomly assigned to a model group, a triptolide group, and three KCR dosage groups (200, 400, 800 mg/kg). Oral administration began on day 10 post-immunization and continued daily until day 30. The model group received 0.3% CMC-Na (same volume as test groups), the triptolide group received 1.0 mg/kg triptolide solution, and KCR groups received corresponding dosages.

Clinical Evaluation

Hind paw thickness and body weight of rats were measured every 3 days using a vernier caliper and electronic balance, respectively. Paw swelling was scored on a 0–4 scale: 0 = no redness/swelling; 1 = red spots or mild toe joint swelling; 2 = red spots with moderate toe joint swelling; 3 = paw swelling; 4 = severe swelling involving ankle joints.

Western Blotting Analysis of Paw Tissues

Rats' hind paws were frozen in liquid nitrogen and ground into powder, which was transferred to pre-cooled 2 mL EP tubes containing RIPA lysis buffer with PMSF and phosphatase inhibitors. After 45 min on ice, lysates were centrifuged at 12,000 rpm for 20 min at 4°C. Supernatants were collected, and total protein was quantified using a BCA assay. Proteins were separated by SDS-PAGE (12%, 10%, 8%, or 6% gels based on molecular weight), transferred to PVDF membranes, and blocked with 5% skim milk. Membranes were incubated with primary antibodies against TNF-α, IL-1β,

IL-6, or β-actin, washed 4 times, and probed with secondary antibodies for 2 h at room temperature. Protein expression was visualized via Tanon imager and quantified using Image J.

Radiologic Analysis

After sampling the rats, we observed bone destruction in the hind paws of each rat using PerkinElmer Micro-CT (MA, USA). Each rat underwent an evaluation for smoothness and presence of osteophytes on the hind paw joint surface using a score ranging from 0 to 4. A score of 0 indicates a smooth surface with no osteophytes, while a score of 1 indicates a slightly rough surface with minimal osteophytes. A score of 2 indicates a rough surface with moderate osteophytes, while a score of 3 indicates a markedly rough surface with significant osteophytes. Finally, a score of 4 indicates a severely rough surface with severe osteophytes. Radiographic scoring was performed on both hind paws of the rats, with a maximum score of 8 per rat.

Histopathological Observation

After sacrifice, hind paws of rats were fixed in 4% paraformaldehyde and decalcified in 10% EDTA solution. Following decalcification, tissues were paraffin-embedded, sectioned, and stained with hematoxylin and eosin (H&E) or Masson's trichrome. Sections were observed under an Olympus fluorescence microscope (Olympus, Tokyo, Japan) at 200× magnification. Masson staining was quantitatively analyzed using Image J. Synovitis was scored based on three parameters: mesenchymal cell activation, inflammatory cell infiltration, and endothelial cell proliferation, each rated 0 (normal) to 3 (severe). Total scores were categorized as: 0–1: normal; 2–3: mild synovitis; 4–6: moderate synovitis; 7–9: severe synovitis.[18,19]

Blood Sample Collection and Indicator Measurement

In order to comprehensively evaluate the therapeutic efficacy of KCR in AIA rats, plasma samples were obtained from all rats on days 21 and 30 following AIA induction for haematological and biochemical analyses.

Gut Microbiology Detection

Following euthanasia, rats were dissected on an ultra-clean bench. The small intestine was excised, and intestinal wall contents were washed with sterile saline. Intestinal mucosa was scraped using a sterile slide under aseptic conditions. For gut microbiota profiling, operational taxonomic unit (OTU) analysis was performed: sequences with ≥97% identity were clustered into OTUs, and chimeric sequences were removed using UCHIME.

Gut Microbiology Analysis

Intestinal microbial analysis was performed by taking intestinal contents of rats (n=5 per group, consistent across normal, model, and KCR treatment groups). The flora contained in the intestinal contents of the rats were analyzed for species composition, diversity, species differences and marker species, and the adequacy of the sample sequences was also evaluated using sparse curves.

Safety Evaluation Analysis

A total of 40 male and female ICR mice were randomly divided into two groups: a control group and a KCR treatment group, with identical treatment protocols applied within each sex. The KCR group received an oral dose of 3000 mg/kg KCR, administered in two aliquots 6 hours apart within a 24-hour period. In contrast, the control group received an equivalent volume of 0.3% CMC-Na vehicle solution over the same 24-hour interval.

All mice were continuously monitored for clinical signs of toxicity, including changes in behavior, mobility, and appearance. Body weights were recorded every two days to assess overall health status. On day 12 post-treatment, mice were euthanized. Blood samples were collected for routine hematological and biochemical analyses, while the liver and spleen were excised to calculate organ indices (organ weight/body weight×100). Additionally, heart, liver, spleen, lung, kidney, stomach, and intestine tissues were harvested, processed, and stained with H&E. Microscopic examination of these tissues was performed to detect any pathological alterations indicative of toxicity in major organs.

Statistical Analysis

The mean and standard deviation were presented for the data. The experiment was conducted independently at least 5 times. Statistical analysis was performed using SPSS 22.0. Single comparisons were analyzed using Student's *t*-test, while multiple comparisons were analyzed using one-way analysis of variance (ANOVA). Statistical significance was considered at $p < 0.05$ and $p < 0.01$.

Results

Identification of KCR-Related Targets and RA-Related Targets

After removing duplicates, 474 KCR targets were obtained from the Pharmmapper, Swiss Target Prediction, and Super-PRED databases. In addition, a total of 6101 RA targets were obtained from the above databases.

Construction of KCR-RA Intersection Targets Network

A total of 466 nodes were found in the PPI network, as shown in Figure S1A. These targets were screened respectively according to degree value, betweenness centrality (BC), and closeness centrality (CC). There were 77 targets with average BC (0.004), CC (0.410), and degree values higher than the average (8), as shown in Figure S1B. The identified targets include AKT1, EGFR, TNF, TP53, ESR1, STAT3, BCL2, CASP3, JUN, etc. 325 common targets (Figure S1C) were screened based on the Venn diagram, and the diagram of a KCR-RA-targets network (Figure S1D) was utilized using Cytoscape software, showing a total of 324 nodes (Figure S1E). The 60 key targets for KCR treatment of RA were identified as AKT1, EGFR, TNF, TP53, ESR1, STAT3, BCL2, CASP3, JUN, etc. (Figure S1F).

KEGG and GO Analysis of KCR-RA Intersection Targets

KEGG and GO enrichment analysis revealed that key pathways involved in RA include the P13K-Akt signaling pathway, MAPK signaling pathway, Ras signaling pathway, etc. (Figure S2A–D).

HPLC-DAD Analysis of Isolated Compounds in the Extract Roots of KCR

HPLC-DAD fingerprinting of KCR root ethanol extract identified eight major compounds (Compounds 1–8; full chemical names are provided in Figure legend) (Figure 1). These compounds are predominantly triterpenes and lignans.

Identification of KCR Major Compound-Related Targets and RA-Related Targets

After removing duplicates, 274 KCR major compound targets were obtained from the Pharmmapper, Swiss Target Prediction, and Super-PRED databases. In addition, a total of 6101 RA targets were obtained from the above databases.

Construction of Major Compounds-RA Intersection Targets Network

A total of 263 nodes were found in the PPI network, as shown in Figure 2A. These targets were screened respectively according to degree value, BC, and CC. There were 47 targets with average BC (0.004), CC (0.410), and degree values higher than the average (8), as shown in Figure 2B. The top 10 identified targets include TNF, G3K3B, EGFR, PIK3CA, PTGS2, MAPK3, MDM2, ESR1, BCL2, and MMP9. 198 common targets (Figure 2C) were screened based on the Venn diagram, and the diagram of a compound 1-8-RA-targets network (Figure 2D) was utilized using Cytoscape software, shows a total of 198 nodes (Figure 2E). The 35 key targets and for compounds 1–8 treatment of RA were identified in Figure 2F, with the top 10 including TNF, EGFR, BCL2, PTGS2, GSK3B, SIRT1, SRC, MTOR, ESR1, and PPARG (Table 1).

KEGG and GO Analysis of KCR Major Compounds-RA Intersection Targets

The top 10 enriched GO terms and the top 20 enriched KEGG pathways are shown in Figure S3. Among the top 20 enriched KEGG pathways related to inflammation were PI3/AKT signaling pathway, apoptosis, T cell receptor signaling pathway, and EGFR signaling pathway (Figure S3A). In the GO enrichment analysis, results related to inflammatory responses in the top ten rankings of the biological processes (BP) analysis encompassed regulation of inflammation

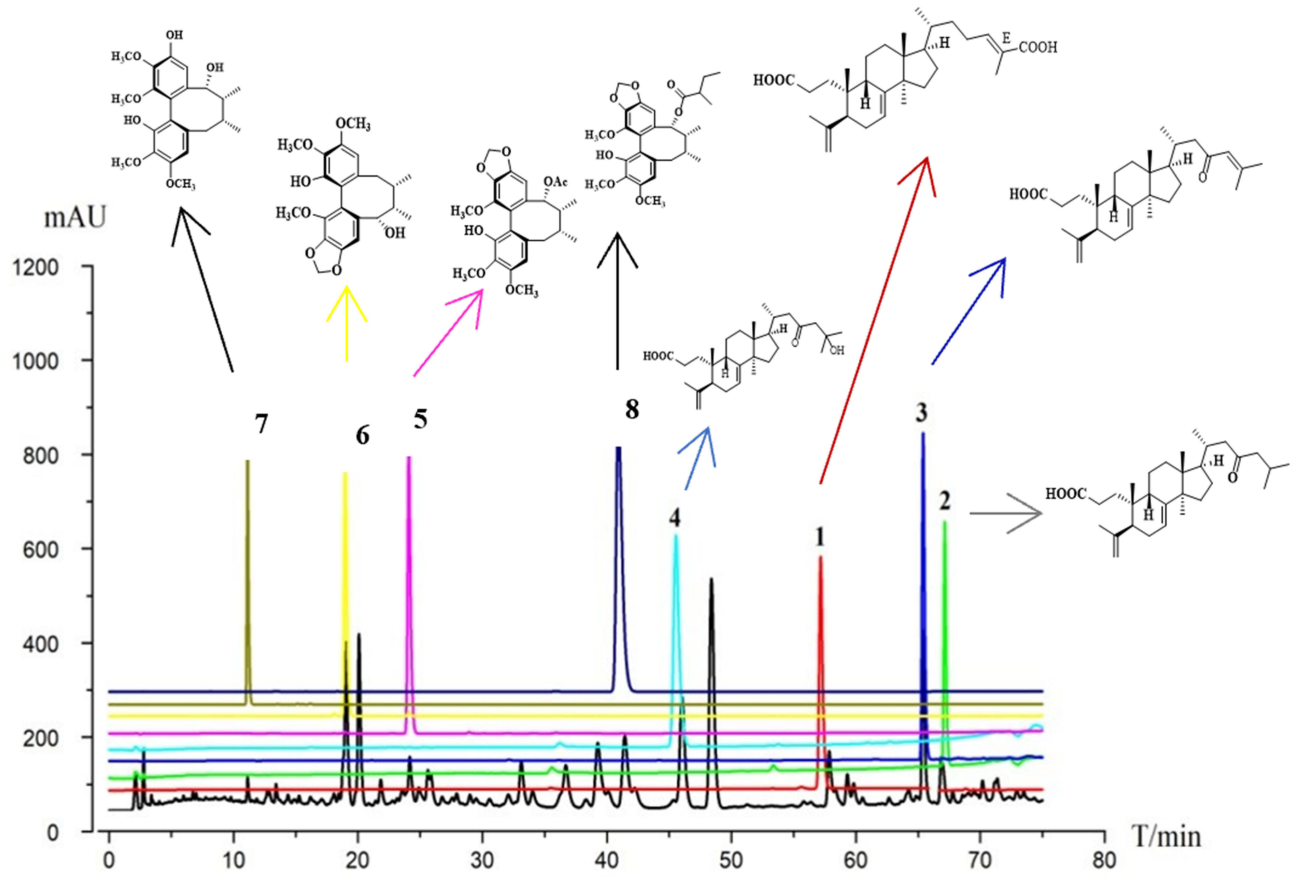

Figure 1 HPLC fingerprint chromatogram of KCR root ethanol extract (horizontal axis: retention time T/min, 0–80 min; vertical axis: absorbance response mAU, 0–1200). Numbered characteristic peaks (linked to structures via directional arrows) correspond to 8 identified compounds: 1. Acetylbinankadsurin A, 2. Binankadsurin A, 3. Isovaleroylbinankadsurin A, 4. seco-coccinic acid A, 5. seco-coccinic acid C, 6. seco-coccinic acid B, 7. 24(E)-3,4-seco-9βH-lanosta-4(28),7,24-triene-3,26-dioic acid (2), 8. Deneolylschisantherin F.

responses, response to oxidative stress, and response to LPS (Figure S3B). In addition, molecular functional (MF) and cellular component analyses revealed that these targets were mainly enriched for nuclear receptor activity and membrane raft (Figure S3C and D).

Molecular Docking Simulation of TNF-α

Compounds 1–8 and the TNF-α protein underwent molecular docking studies. Lower binding free energies implied a more stable conformation and a stronger affinity for protein receptor, potentially enhancing inhibitory activity. The compounds and TNF-α showed promising binding energies, scoring −6.40, −8.30, −7.13, −4.28, −4.23, −4.58, −4.80, and −4.03 kcal/mol, respectively. In the end, by observing the effects of all compounds on the interaction between the hydrogen bonds and hydrophobic bonds of amino acid residues in TNF-α, it was found that the hydrogen bonds play a dominant role in this binding mode (Table 2). Compound 2 displayed the lowest binding free energy with nine amino acid residues of the enzyme. The hydrogen bonding interaction between the compounds and the amino acid residues of TNF-α were represented visually in Figure 3.

KCR Inhibited the Expression of Inflammatory Protein in RAFLS Cells and RAW264.7 Cells

Western blotting was employed to analyze inflammatory proteins, investigating whether KCR inhibits inflammation and proliferation of RAFLS and RAW264.7 cells by regulating key cytokines (TNF-α, IL-1β, IL-6). As illustrated in Figure 4A and B, KCR markedly decreased the expression of TNF-α, IL-1β, and IL-6 in LPS-stimulated RAFLS;

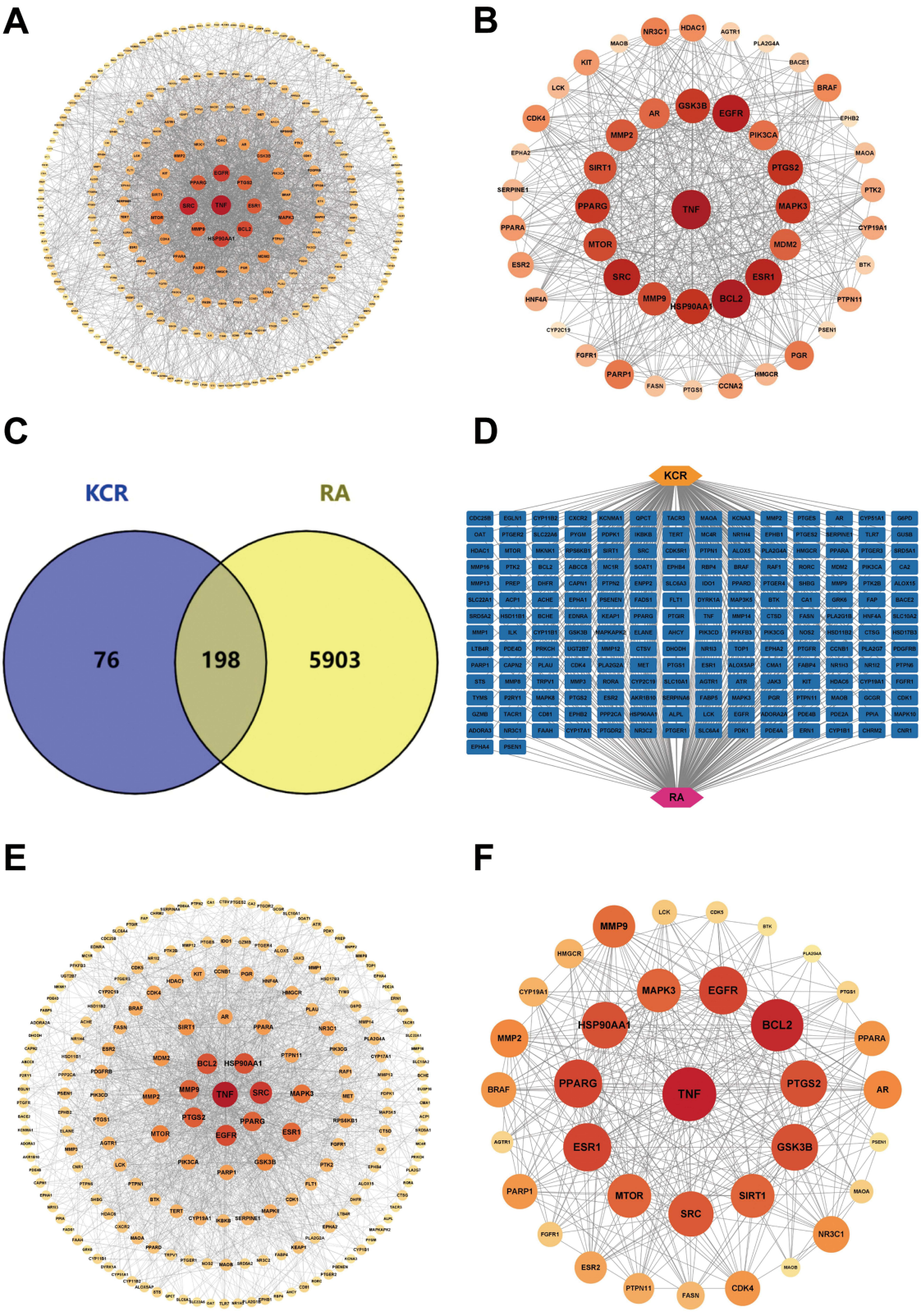

Figure 2 Screening for interacting targets of RA and the major compounds of KCR. (**A**) PPI network of potential therapeutic targets for the major compounds of KCR. (**B**) 47 core targets for the major compounds of KCR had higher than average BC, CC and Degree values. (**C** and **D**) 198 interacting targets between RA and the major compounds of KCR. (**E**) PPI network of RA and the major compounds of KCR. (**F**) PPI network of core targets of the major compounds of KCR for RA.

https://doi.org/10.2147/JIR.S557108

Table 1 Top 10 Targets Ranked by Degree Method in PPI Network

Number	Gene Name	Protein Name	Related Signaling Pathway
1	TNF	Tumor necrosis factor	TNF signaling pathway
2	EGFR	Epidermal growth factor receptor	PI3K/Akt signaling pathway
3	BCL2	B-cell lymphoma-2	Apoptosis signaling pathway
4	PTGS2	Cyclooxygenase-2	Nrf2/ARE signaling pathway
5	GSK3B	Glycogen synthase kinase 3 β	PI3K/Akt signaling pathway
6	SIRT1	Silent mating-typeinformation regulator 2 homolog 1	SIRT1-PGC-1α signaling pathway
7	SRC	SRC proto-oncogene, non-receptor tyrosine kinase	PI3K/Akt signaling pathway
8	MTOR	Mammalian target of rapamycin	mTOR signaling pathway
9	ESR1	Estrogen receptor 1	Estrogen signaling pathway
10	PPARG	Peroxisome proliferator-activated receptor gamma	PPAR signaling pathway

Table 2 Molecular Docking Results of Compounds 1–8 and TNF-α

Compounds	Binding Energy (kcal/mol)	Amino Acid Residues
1	−6.40	GLY134, GLN131, GLN135, GLU141, ASP130, ALA142, ARG138, ARG137, UNK1
2	−8.30	GLY190, ARG137, GLN193, GLY134, ARG129, TRP187, LEU186, LEU133, ASP130
3	−7.13	PRO139, TYR253, TYR249, ARG137, ARG234, VAL231, VAL191, ALA195, LEU235, LEU140, ALA194, ARG138, ARG198, GLU141, GLU197
4	−4.28	GLY134, GLY190, LEU186, ASP130, GLU197, ARG129, ARG138, ARG137, LEU133
5	−4.23	GLY134, GLY190, GLN131, GLN193, ASP130, ASP189, LEU186, ARG129, ARG137, LEU133,
6	−4.58	GLY134, GLY190, GLN131, GLN135, GLN193, LEU136, LEU186, ASP130, ARG129, ARG137, LEU133, TRP187
7	−4.80	GLY190, GLN193, ASP130, ASP189, ARG137, ARG138, TRP187, GLY134, LEU186, LEU133
8	−4.03	GLN131, GLU141, GLU143, ARG137, ARG146, GLY134, GLN135, ARG138, ALA142, UNK1

notably, at concentrations of 0.2 mg/mL and 0.4 mg/mL, KCR reduced the levels of these cytokines to below the baseline of the normal group (Figure 4B). A consistent inhibitory trend was observed in LPS-stimulated RAW264.7 cells (Figure 4C and D), though the reduction did not fall below the normal group baseline in this cell model. This unique trend in RAFLS is associated with the strong regulatory effect of KCR's core active components on the TNF-α-mediated inflammatory pathway, the key pro-inflammatory axis driving RAFLS activation. Collectively, these findings suggest that the anti-RA activity of KCR is closely linked to its suppression of inflammatory proteins in synovial fibroblasts and inflammatory macrophages, with high-dose KCR exerting a more potent regulatory effect on RAFLS-derived inflammatory cytokines.

KCR Suppresses Paw Edema and Arthritic Manifestations in AIA Rats

Nine days post-AIA induction, pronounced paw erythema and swelling were observed in both the model and treatment groups. Relative to normal rats, AIA-induced rats exhibited markedly impaired body weight gain (Figure 5A). Importantly, KCR treatment conferred a dose-dependent therapeutic benefit: AIA rats receiving KCR displayed restored body weight gain trajectories and significant attenuation of paw swelling (Figure 5B–D), indicating improved systemic health status.

KCR Ameliorates Bone Destruction and Pathological Lesions in AIA Rats

Micro-CT imaging of rat paws showed that AIA rats exhibited prominent osteophyte formation and bone erosion compared to normal controls, findings that were significantly ameliorated in the KCR treatment group (Figure 6A and C). H&E staining revealed joint space narrowing, aggressive synovial hyperplasia, and inflammatory cell infiltration in AIA rats (Figure 6B and D). Masson' s trichrome staining further showed heterogeneous cartilage superficial layer staining, pronounced fibrosis, and intense red staining near tidemarks. Histopathological changes demonstrated a dose-

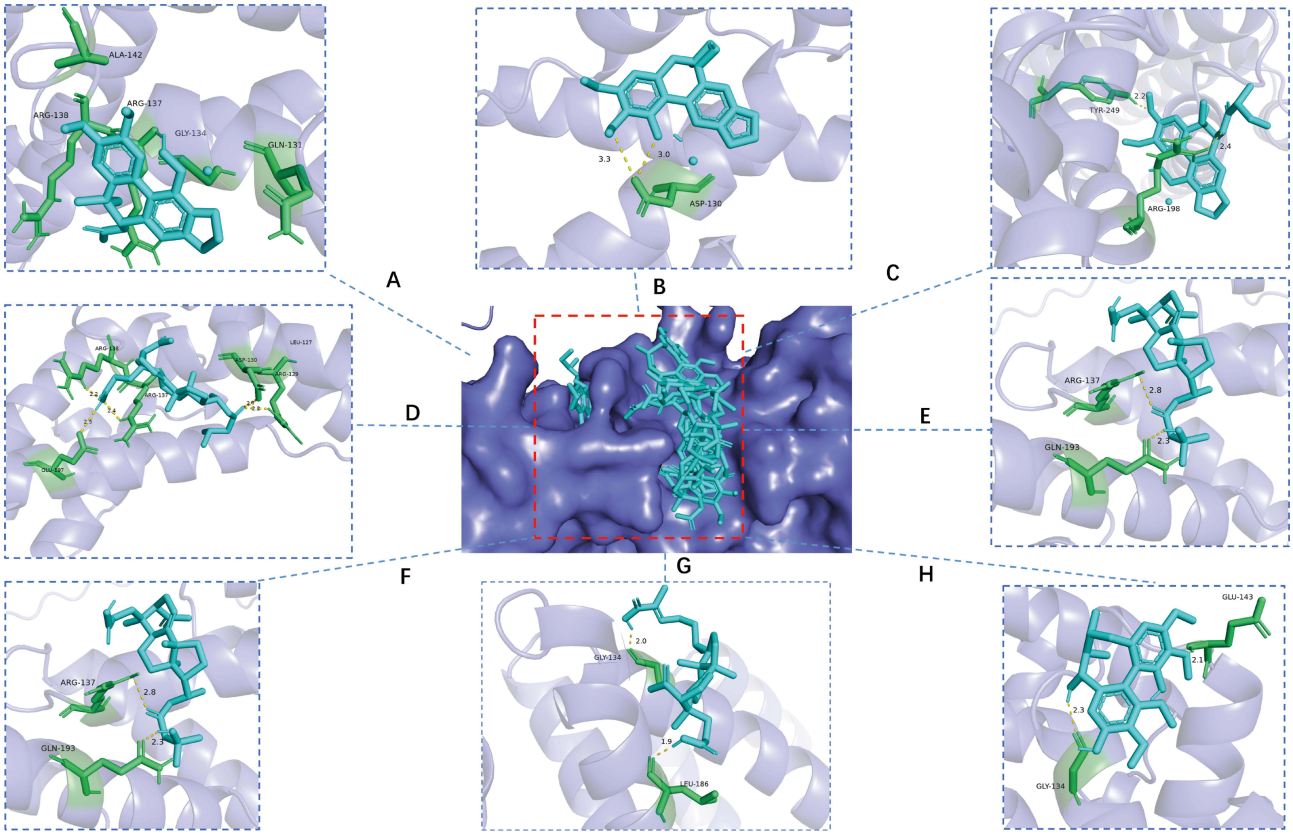

Figure 3 Validation of binding between the major compound of KCR and TNF-α. (**A**–**H**) Docking predictions of KCR's major compounds 1–8 with TNF-α, respectively. Compound 1: Acetylbinankadsurin A, Compound 2: binankadsurin A, Compound 3: Ilsovaleroylbinankadsurin A, Compound 4: seco-coccinic acid A, Compound 5: seco-coccinic acid C, Compound 6: seco-coccinic acid B, Compound 7: 24(E)-3,4- seco-9βH-lanosta-4(28),7,24-tirene-3,26-dioic acid (2), Compound 8: Deaneoloylschisantherin F. The central panel (**G**) shows the surface model of TNF-α, where the red dashed box specifically designates the binding pocket region.

dependent improvement with KCR treatment: at 800 mg/kg, joint space regained a normal appearance with absent synovial hyperplasia or inflammatory infiltration. Articular cartilage exhibited uniform staining, minimal fibrosis, and no red staining near tidemarks (Figure 6B and E). These in vivo results collectively demonstrate KCR's therapeutic potential to alleviate joint pathology and improve systemic health in AIA rats, highlighting its promise as a candidate therapeutic for RA.

KCR Suppresses Pro-Inflammatory Cytokines in AIA Rats

Consistent with in vitro results, Western blotting analysis revealed up-regulation of TNF-α, IL-1β, and IL-6 in paw tissues of AIA rats. Conversely, KCR treatment significantly reduced the expression of these cytokines in paw tissues (Figure 7A and B). These findings indicate that KCR exerts therapeutic effects in RA by regulating TNF-α-mediated inflammatory pathways.

KCR Modulates Hematological Parameters in AIA Rats

Plasma samples were collected from rats on days 21 and 30 for comprehensive biochemical and haematological analyses. Biochemical assays focused on liver function markers (ALT, γ-GT, LDH), lipid profiles (TG), and renal function indices (UREA). Results showed significantly compromised liver and kidney functions and reduced lipid levels in AIA rats compared to the normal group. Notably, KCR treatment at specific doses restored liver/kidney functions and regulated blood lipids in AIA rats (Figure S4A). Routine blood analyses further revealed that AIA-induced rats exhibited abnormally elevated inflammatory cell counts, diminished hematopoietic function, and increased PLT levels compared to controls. Remarkably, KCR treatment reversed these hematological abnormalities, leading to decreased inflammatory

https://doi.org/10.2147/JIR.S557108

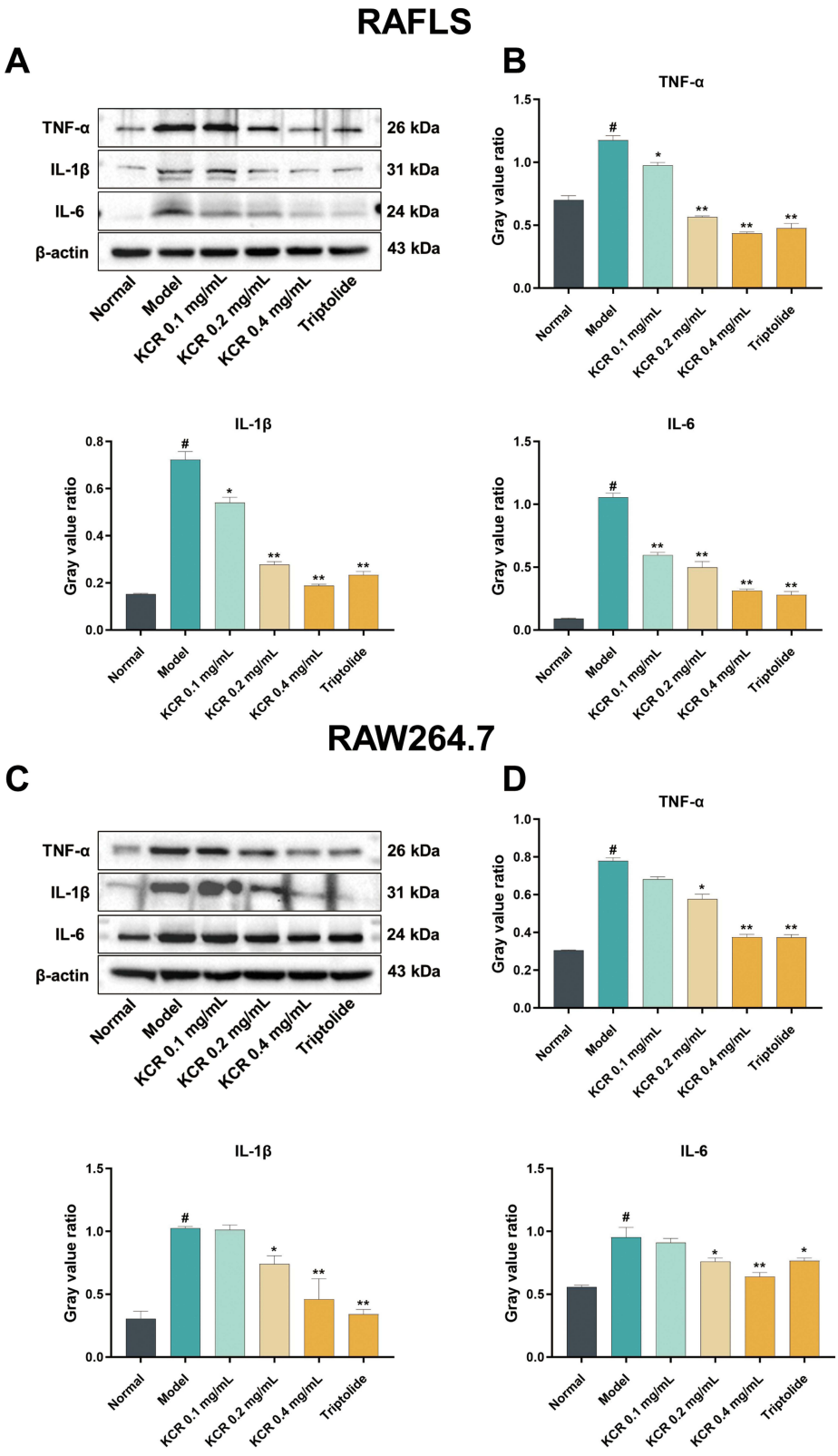

Figure 4 KCR inhibits the expression of inflammatory protein in LPS-induced RAFLS and RAW264.7 cells. (**A**) Expression of TNF-α, IL-1β and IL-6 proteins in LPS-induced RAFLS in each group. (**B**) Quantitative analysis of gray values of TNF-α, IL-1β, and IL-6 proteins in LPS-induced RAFLS. (**C**) Expression of TNF-α, IL-1β and IL-6 proteins in LPS-induced RAW264.7 cells in each group. (**D**) Quantitative analysis of gray values of TNF-α, IL-1β, and IL-6 proteins in LPS-induced RAW264.7 cells. * $p < 0.05$, ** $p < 0.01$ vs. the Normal group, # $p < 0.05$ vs. the Model group.

https://doi.org/10.2147/JIR.S557108

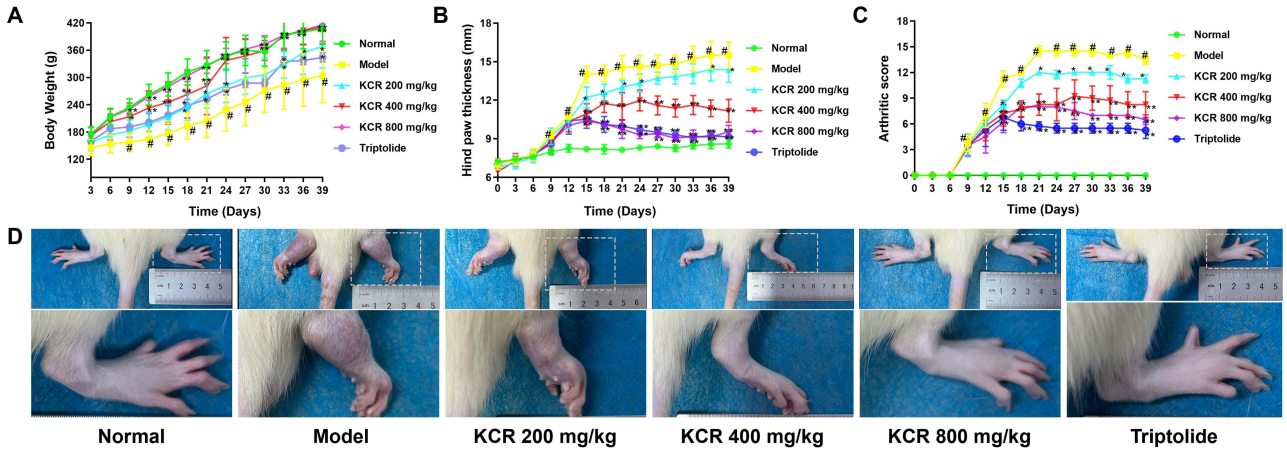

Figure 5 The therapeutic effects of KCR on AIA rat model. (**A**) Weight change curve of rats. (**B**) Swelling thickness of rat foot and paw. (**C**) Arthritis score of rats. (**D**) Images of rat paw. * $p < 0.05$, ** $p < 0.01$ vs. the Normal group, # $p < 0.05$ vs. the Model group.

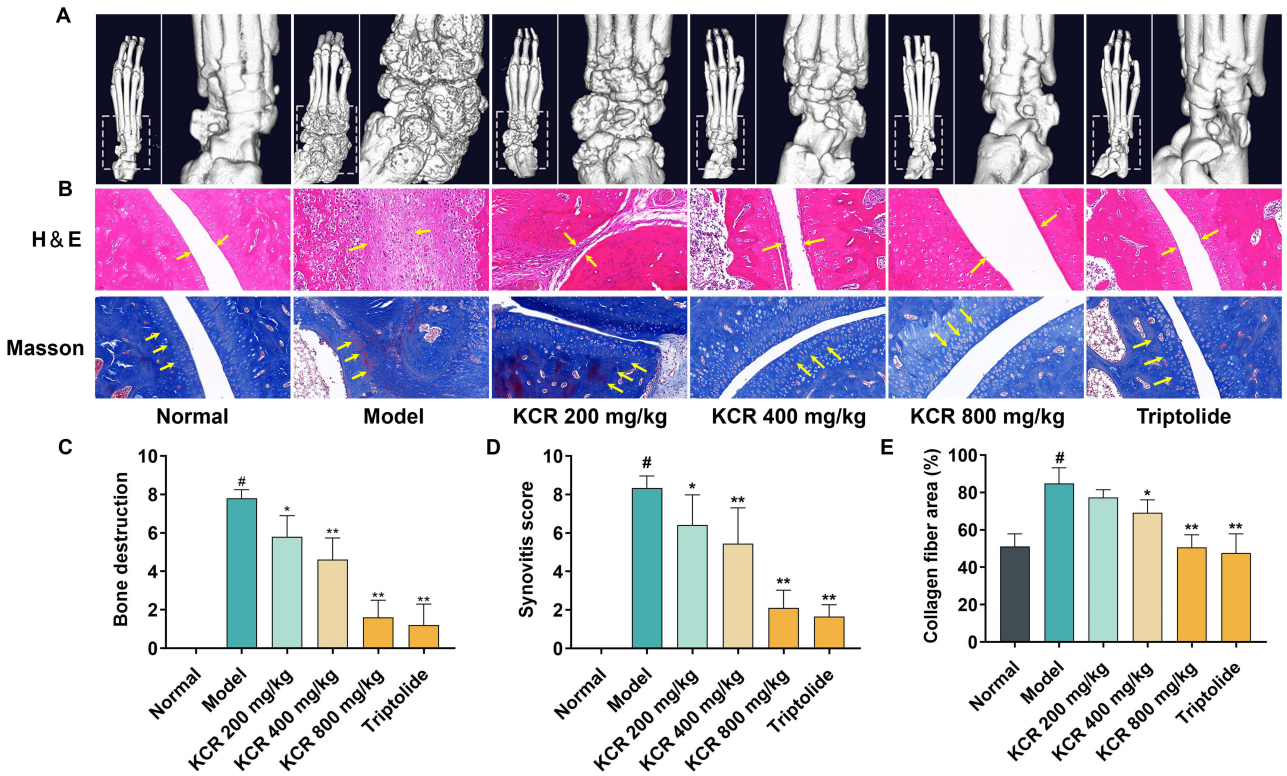

Figure 6 In vivo osteoprotective and histopathological modulation effects of KCR in AIA rat model. (**A**) Microscopic CT image of rat foot paw. (**B**) H&E and Masson staining images of rat foot paws (200×); the yellow arrows indicate corresponding pathological changes in tissue sections (in H&E staining: inflammatory cell infiltration and synovial hyperplasia; in Masson staining: collagen fibrosis accumulation). (**C**) Scoring of bone destruction in rat foot paw. (**D**) Scoring of synovitis in rat paws. (**E**) Quantification of collagen fibrosis in rat paws. * $p < 0.05$, ** $p < 0.01$ vs. the Normal group, # $p < 0.05$ vs. the Model group.

cell proportions, improved hematopoiesis, and normalized PLT levels (Figure S4B). Collectively, these blood-based analyses highlight KCR's multifaceted therapeutic effects in AIA rats, demonstrating its capacity to ameliorate impaired organ functions and resolve dysregulated inflammatory-hematopoietic profiles.

Following euthanasia, the liver, spleen, and thymus of rats in each group were dissected and weighed to calculate organ indices (organ weight/body weight × 100), which were used to assess KCR's effect on organ alterations in AIA rats. Results showed that AIA immunization significantly increased liver, spleen, and thymus indices, whereas KCR

https://doi.org/10.2147/JIR.S557108

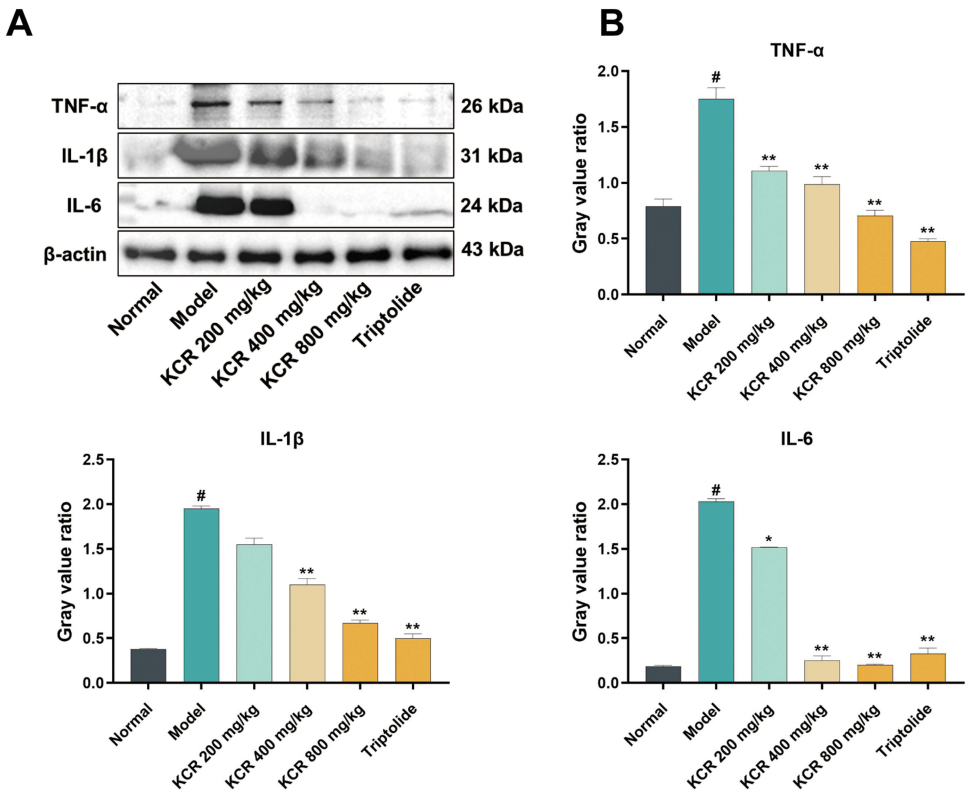

Figure 7 KCR-mediated suppression of TNF-α and pro-inflammatory cytokines in AIA rats. (**A**) Expression of TNF-α, IL-1β and IL-6 proteins in AIA rats in each group. (**B**) Quantitative analysis of gray values of TNF-α, IL-1β, and IL-6 proteins in AIA rats. * $p < 0.05$, ** $p < 0.01$ vs. the Normal group, # $p < 0.05$ vs. the Model group.

treatment normalized these indices in a dose-dependent manner (Figure S4C–E). These findings further validate KCR's potential as a promising therapeutic candidate for RA management.

Taxonomic Composition Analysis of Gut Microbiota

Taxonomic composition analysis of the gut microbiota was conducted at the phylum (Figure S5A) and genus (Figure S5B) levels, focusing on the top 10 most abundant taxa. The rarefaction curves of the gut content samples from each group reached a plateau, indicating that the sequencing depth was sufficient to capture the microbial diversity within the samples (Figure S5C).

Gut Microbiota Diversity Profiling and Modulation by KCR

Alpha diversity of the gut microbiota was assessed using richness (Chao1, Observed ASVs) and evenness (Pielou's evenness) indices, as well as diversity metrics (Shannon, Simpson). A Venn diagram illustrated unique and shared microbial OTUs across groups (Figure 8A). Compared to normal rats, AIA rats showed significant reductions in microbial richness, evenness, and diversity. Notably, KCR treatment dose-dependently restored these parameters, suggesting microbiota-mediated therapeutic effects (Figure 8B). Beta diversity analysis via principal coordinate analysis (PCoA) based on Bray–Curtis distances revealed distinct microbial community structures. AIA rats exhibited significantly lower community similarity to normal controls, while KCR-treated rats showed microbiota composition resembling normal groups and deviating from AIA patterns (Figure 8C). This indicates KCR's role in reshaping gut microbial architecture. Differential abundance analysis identified distinct microbial profiles between normal/AIA and KCR/AIA groups (Figure 8D). AIA rats showed reduced microbial diversity and increased *Corynebacterium* abundance, both reversed by KCR. Mechanistically, TNF-α-mediated disruption of gut barrier integrity and pro-inflammatory microbial shifts were attenuated by KCR, suggesting that TNF-α inhibition restores microbial homeostasis.

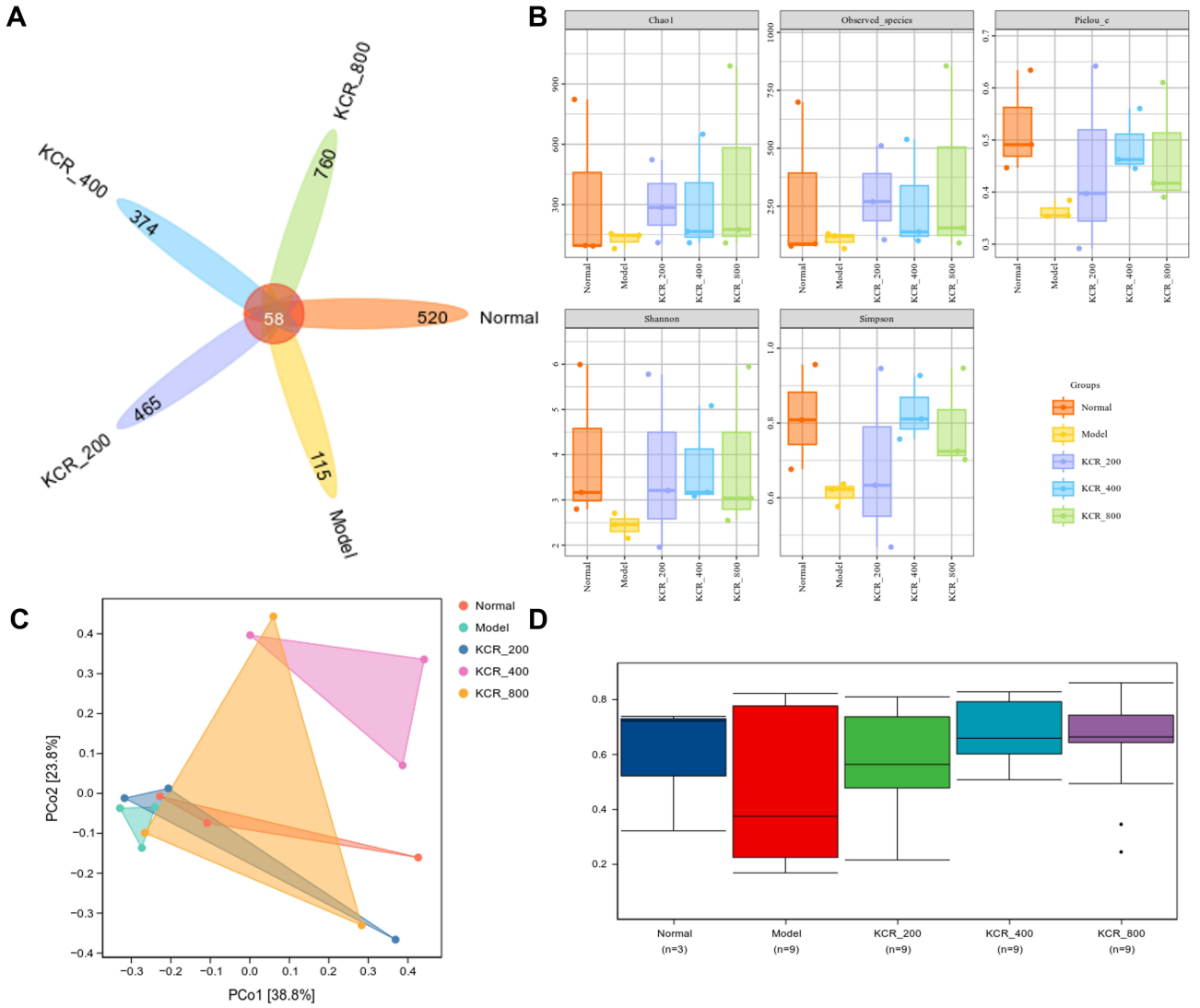

Figure 8 Gut microbiota diversity modulation and community analysis in AIA rats. (**A**) Venn plots of the number of unique and shared species in each group. (**B** and **C**) Alpha diversity and beta diversity analyses of gut microbiota in AIA rats. (**D**) Differential abundance analysis of gut microbiota in AIA rats.

Species Variation and Marker Species Analysis

Gut microbiome composition differences and key taxon identification across experimental groups were analyzed using a heatmap to visualize taxonomic profile similarities/differences (Figure S6A), where vertical clustering reflected inter-sample similarity in microbial abundance (shorter branches indicating higher similarity) and horizontal clustering showed intra-sample similarity for each taxon (shorter branches denoting closer abundance correlation). Random forest analysis identified the top 20 taxa driving community variation, highlighting *Corynebacterium* and *Jeotgalicoccus* as key differentially abundant genera (Figure S6B). These taxa interact with TNF-α signaling: *Corynebacterium* exacerbates inflammation via TNF-α induction, while KCR suppresses this feedback loop—correlating with reduced *Corynebacterium* abundance in treated groups. The identified biomarkers align with KCR's dual mechanism of inhibiting TNF-α and restoring microbial homeostasis by modulating taxa involved in TNF-α crosstalk, underscoring the microbiota-TNF-α axis as a potential RA therapeutic target.

In vivo Biosafety Assessment of KCR in Mice

After administering a high dose of KCR (3000 mg/kg), all male and female mice in the KCR group survived the 14-day observation period without abnormal behaviors such as convulsions, diarrhea, or reduced activity. Body weight monitoring showed similar gain trends in male mice of both the KCR and normal groups (Figure 9A), with comparable

https://doi.org/10.2147/JIR.S557108

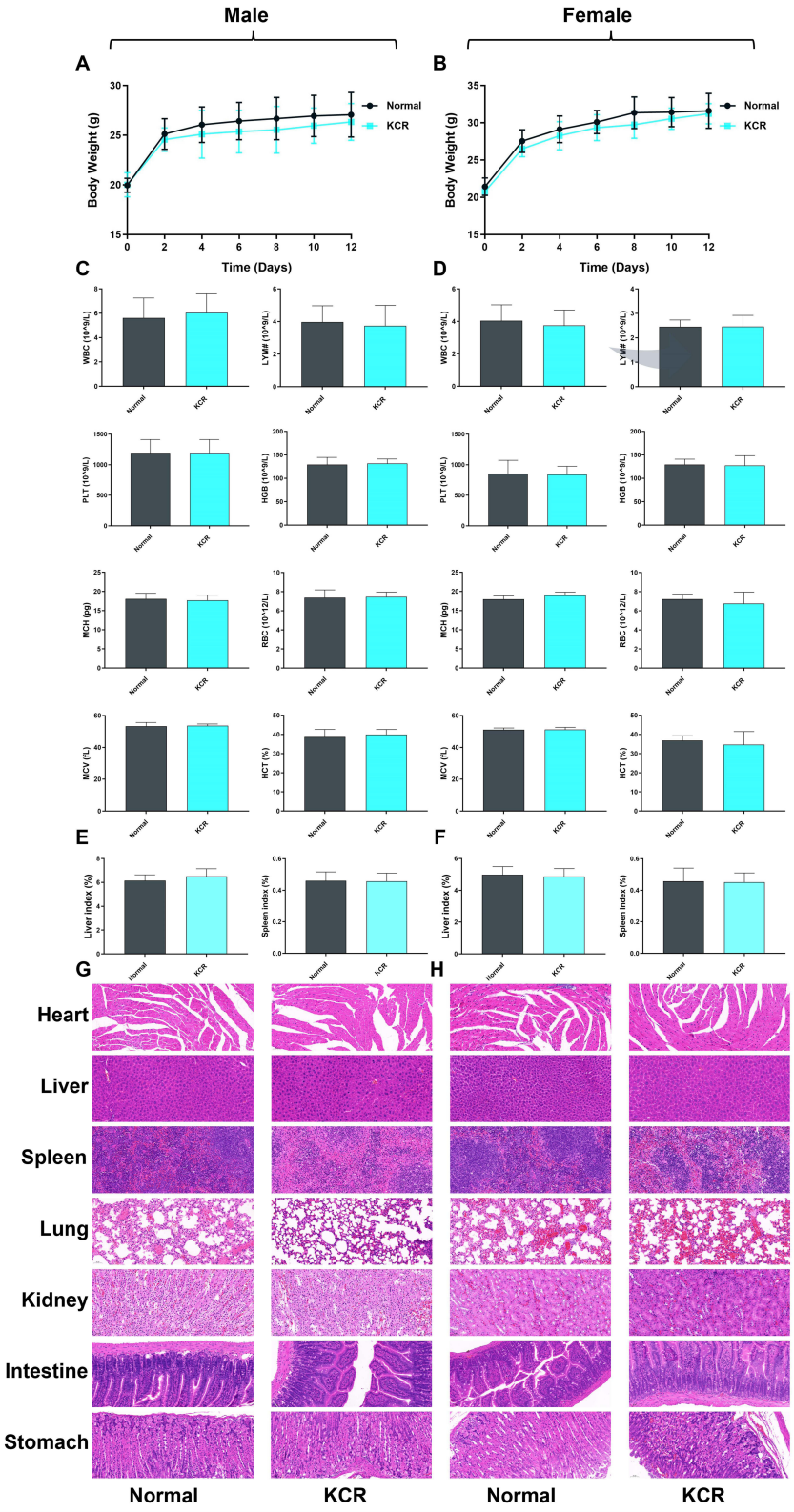

Figure 9 In vivo biosafety profiling of KCR (3000 mg/kg) in male and female mice. (**A** and **B**) Body weight changes of male and female mice in each group over time. (**C** and **D**) Routine blood indices of male and female mice in each group. (**E** and **F**) Organ indices of male and female mice in each group. (**G** and **H**) Histopathological images of Heart, Liver, Spleen, Lung, Kidney, Intestine, and Stomach in male and female mice.

weight changes in female mice (Figure 9B), indicating that high-dose KCR did not impact animal growth. Routine blood analyses revealed no significant differences in hematological parameters (WBC, LYM, PLT, HGB, MCH, RBC, MCV, HCT) between KCR and normal groups in either sex (Figure 9C and D).

H&E staining of major organs showed normal histological features: liver hepatocytes were arranged orderly without steatosis (Figure 9E and F), renal glomeruli were structurally intact with no tubular necrosis, the spleen displayed distinct white and red pulp, and the gastrointestinal tract maintained normal mucosal and muscular layers. Additionally, heart and lung tissues showed no inflammatory infiltration or structural damage (Figure 9G and H). Collectively, these results demonstrate the high in vivo biosafety of KCR.

Discussions

RA is a chronic autoimmune disease characterized by persistent synovial inflammation, leading to progressive joint destruction. Prolonged inflammation drives bone erosion, joint deformity, and eventual disability.[20,21] Moreover, RA is associated with serious comorbidities—including lung diseases, cardiovascular disorders, malignant tumors, and depression—with severe cases posing life-threatening risks. This underscores the urgent need for low-toxicity therapeutic agents to manage RA.[22]

Intestinal inflammation triggered by localized infections, gut dysfunction, or food antigens elicits release of pro-inflammatory cytokines (IFN-γ, IL-1β, IL-6, TNF-α) and immune mediators.[23–25] Unchecked, these factors induce systemic consequences: circulating pro-inflammatory factors compromise barrier integrity (eg, gastrointestinal barrier [GVB], blood-brain barrier [BBB]) by disrupting epithelial tight junctions, leading to increased intestinal permeability ("leaky gut"). Concomitant disruption of central nervous system (CNS) barriers allows intestinal-derived molecules, toxins, and pathogens to access the brain parenchyma, activating local immune cells and triggering neuroinflammation.[26–29] During the pathogenesis of RA, the immune system is abnormally activated, resulting in excessive proliferation and activation of immune cells such as T-cells and macrophages. These activated immune cells secrete a large number of inflammatory factors, such as TNF-α, IL-6, IL-1β, etc., which trigger and maintain the inflammatory response in the joints.[30–34] In addition, an imbalance in the subpopulation of Th cells is an important factor in the exacerbation of the inflammatory response in RA patients. Under normal conditions, there is a balance between cell subsets such as Th1, Th2, Th17 and Treg, which work together to maintain immune homeostasis. However, in RA patients, Th1 and Th17 cell subsets tend to be overactivated, while Treg cell function may be suppressed. This imbalance leads to increased expression of pro-inflammatory factors such as TNF-α and IL-17, and relative under-expression of anti-inflammatory factors such as IL-4 and IL-10, thereby exacerbating the inflammatory response.[35,36]

Network pharmacology predictions and molecular docking simulations suggested that KCR exerts anti-RA effects via TNF-α modulation, with these in silico analyses focusing on the binding potential of individual isolated compounds from KCR (eg, triterpenes, lignans) to key targets such as TNF-α. It is important to note that the present study utilized a total ethanol extract of KCR, and thus the observed effects are likely the result of synergistic action among its multiple bioactive components, rather than the activity of a single constituent. In vitro studies showed that KCR at 0.2 and 0.4 mg/mL significantly inhibited LPS-induced expression of TNF-α, IL-1β, and IL-6 in RAFLS and RAW264.7 cells; in RAFLS specifically, these doses reduced cytokine levels below the normal group baseline (Figure 4B), a phenomenon with biological rationality. The core reason for this is that KCR's integrated active components exert a potent, targeted regulatory effect on the TNF-α signaling pathway, which not only blocks LPS-induced TNF-α overexpression in RAFLS but also fine-tunes the basal TNF-α signaling that synovial fibroblasts inherently rely on to maintain a pro-inflammatory primed state in RA pathogenesis. Future work to isolate and characterize individual constituents of KCR will be critical to dissect their specific contributions to the observed anti-RA and microbiota-modulating effects, and to identify the key active molecules that drive the synergistic regulatory network of the TNF-α-gut microbiota axis. This targeted regulation is unique to RAFLS, reflecting KCR's selective action on the key effector cells of RA joint destruction rather than non-specific immune suppression. Consistently, in AIA rats, KCR ethanol extract at 400 and 800 mg/kg suppressed these inflammatory cytokines in hind paw tissues, indicating TNF-α-mediated anti-inflammatory activity, and validating the translational relevance of this potent synovial inflammation-regulating effect. KCR also demonstrated dose-dependent suppression of paw edema and bone destruction in AIA rats (200–800 mg/kg). Histological analyses (H&E and Masson

staining) revealed that KCR inhibited synovial hyperplasia, inflammatory cell infiltration, and fibrosis in hind paw joints. Systemic evaluations showed KCR restored hematological parameters (liver/kidney function, lipid metabolism) compromised by AIA.

Notably, administration of a high KCR dose (3000 mg/kg) did not induce acute toxicity in mice, as corroborated by unremarkable body weight gain curves, stable hematological parameters (WBC, LYM, and PLT counts), and histologically intact architecture of major organs (liver, kidney, and spleen) devoid of inflammatory infiltrates or degenerative lesions. These observations validate the in vivo safety of KCR and bolster its translational applicability for RA therapeutic intervention.

Gut microbiota analyses revealed that AIA rats exhibited reduced intestinal microbial diversity and increased *Corynebacterium* spp. abundance compared to normal controls, indicating potential dysbiosis associated with RA pathogenesis. Preclinical studies have confirmed that targeted depletion of *Corynebacterium* can alleviate paw swelling and bone destruction in AIA rats by reducing systemic TNF-α secretion, while clinical cohorts have validated that *Corynebacterium* overgrowth is positively correlated with synovial TNF-α levels and joint erosion scores.[37] Conversely, KCR-treated AIA rats showed restored gut microbial diversity and reduced *Corynebacterium* abundance, suggesting a role for *Corynebacterium* spp. in driving inflammatory pathogenesis in AIA. This aligns with our network pharmacology and molecular docking results, which demonstrated strong binding affinity between KCR components and TNF-α (eg, Compound 2, ΔG=−8.30 kcal/mol). As TNF-α disrupts intestinal epithelial tight junctions to induce dysbiosis, KCR's inhibitory effect on TNF-α not only reduces synovial tissue inflammation but also reverses microbial imbalance—including the suppression of *Corynebacterium* overgrowth. Collectively, these findings suggest a potential mechanistic link between KCR's anti-RA effects, inflammation inhibition, and gut microbiota modulation (Figure 10). It is important to note that the binding interactions between KCR-derived compounds and TNF-α were solely predicted by molecular docking simulations in this study, without complementary

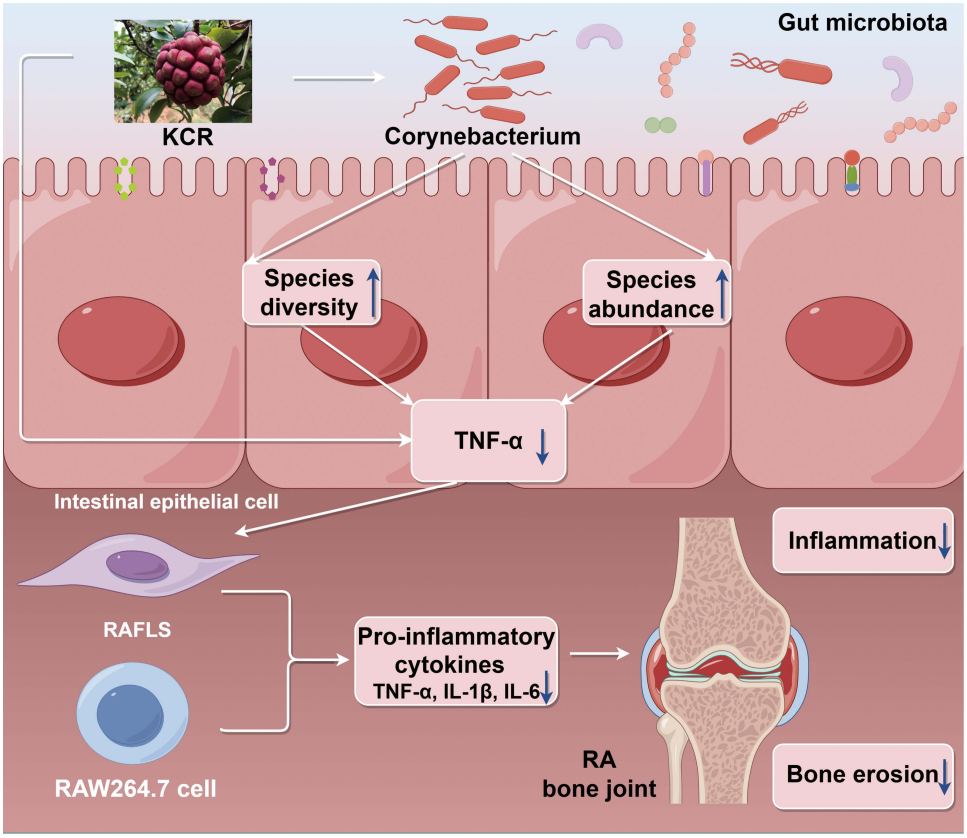

Figure 10 Schematic of KCR's mechanism via the TNF-α-gut-immune-joint axis. KCR suppresses TNF-α to reduce synovial inflammation and modulates *Corynebacterium* to restore gut homeostasis, forming a reciprocal regulatory loop (↓= decrease; ↑= increase). This Fig. was drawn using Figdraw (https://www.figdraw.com), export ID: SSOSP6e7f5.

biophysical validation such as surface plasmon resonance (SPR) assays or molecular dynamics simulations to confirm binding affinity and dynamic stability. This represents a limitation that should be addressed in future research.

Conclusion

Collectively, this study suggests the TNF-α–gut microbiota axis as the pivotal mechanism underlying KCR's anti-RA efficacy: KCR alleviates joint pathology in vivo, suppresses inflammatory responses, and modulates gut microbiota (eg, *Corynebacterium*) by targeting TNF-α, integrating dual therapeutic effects that distinguish it from current RA treatments which often focus solely on anti-inflammation. These findings highlight KCR's potential as an ethnomedicine-based candidate for RA, providing a preclinical foundation for its translational development.

Notably, this work has limitations: further clinical trials are required to validate efficacy, safety, and optimal dosing in humans. Additionally, the specific microbial metabolites mediating KCR's anti-RA effects warrant future investigation. Despite these, the study elucidates a novel multi-target mechanism for KCR and supports the development of microbiota-modulating anti-RA therapeutics, expanding the translational potential of ethnomedicines in autoimmune disease management.

Abbreviations

ACPA, Anti-citrullinated protein antibodies; AIA, Adjuvant-induced arthritis; BBB, Blood-brain barrier; BC, Betweenness centrality; BP, Biological processes; CC, Closeness centrality; CFA, Complete Freund's adjuvant; CNS, Central nervous system; DAD, Diode array detector; DMSO, Dimethyl sulfoxide; EDTA, Ethylenediaminetetraacetic acid; FBS, Fetal bovine serum; GO, Gene ontology; GVB, Gastrointestinal barrier; HPLC, High performance liquid chromatography; H&E, Hematoxylin and eosin; IL-1β, Interleukin-1β; IL-6, Interleukin-6; KCR, The root of *Kadsura coccinea* (Lem.) A. C. Smith; KEGG, Kyoto encyclopedia of genes and genomes; LPS, Lipopolysaccharide; Masson, Masson's trichrome; NF-κB, Nuclear factor kappa-B; OUT, Operational taxonomic unit; PMSF, Phenylmethylsulfonyl fluoride; PPI, Protein-protein interaction; RA, Rheumatoid arthritis; RAFLS, Rheumatoid arthritis fibroblast-like synoviocytes; RF, Rheumatoid factor; SD, Standard deviation; SPF, Specific pathogen-free; TNF-α, Tumor necrosis factor-α.

Data Sharing Statement

The data generated and analyzed in this study are available from the corresponding author (Wei Wang) upon reasonable request.

Ethical Approval

The experiment was conducted in accordance with the Regulations on the Administration of Laboratory Animals after being reviewed by the Animal Ethics Committee of Hunan University of Chinese Medicine (permit number: 202302190001). For the plant material involved in this study, it was formally identified by botanist Wei Wang. In accordance with the institutional regulations of Hunan University of Chinese Medicine and local relevant provisions, no additional approval is required for the research involving this plant material.

Author Contributions

All authors made a significant contribution to the work reported, whether that is in the conception, study design, execution, acquisition of data, analysis and interpretation, or in all these areas; took part in drafting, revising or critically reviewing the article; gave final approval of the version to be published; have agreed on the journal to which the article has been submitted; and agree to be accountable for all aspects of the work.

Funding

This work was supported by Natural Science Foundation of China (82204766, 82304878, 82174078); Changjiang Scholars Program in Ministry Education, People's Republic of China (T2019133); Xiaohe Sci-Tech Talents Special Funding under Hunan Provincial Sci-Tech Talents Sponsorship Program (2023TJ-X71); Natural Science Foundation of Hunan province (2023JJ40490, 2023JJ30445); Science and Technology Innovation Program of Hunan Province (2024RC3201); Hunan University of Chinese Medicine Pharmacy first-class construction Discipline Project;

Outstanding Youth Program of Hunan University of Chinese Medicine (202202); The Scientific Research Fund of Hunan University of Chinese Medicine (2021XJJJ006); Open Foundation Project of Hunan International Joint Laboratory of Traditional Chinese Medicine (2022GJSYS02); Changsha Outstanding Innovative Youth Training Program (kq2306021); Undergraduate Research and Innovation Foundation of Hunan University of Chinese Medicine (2023098); Research Foundation of Education Bureau of Hunan Province (24C0627). Undergraduate Research and Innovation Foundation of Hunan University of Chinese Medicine (2024BKS083).

Disclosure

The authors declare that they have no known competing financial interests or personal relationships that could have appeared to influence the work reported in this article.

References

1. Cush JJ. Rheumatoid arthritis: early diagnosis and treatment. *Rheum Dis Clin North Am*. 2022;48(2):537–547. doi:10.1016/j.rdc.2022.02.010
2. Finckh A, Gilbert B, Hodkinson B, et al. Global epidemiology of rheumatoid arthritis. *Nat Rev Rheumatol*. 2022;18(10):591–602. doi:10.1038/s41584-022-00827-y
3. Abbasi M, Mousavi MJ, Jamalzehi S, et al. Strategies toward rheumatoid arthritis therapy; the old and the new. *J Cell Physiol*. 2019;234(7):10018–10031. doi:10.1002/jcp.27860
4. Lin YJ, Anzaghe M, Schülke S. Update on the pathomechanism, diagnosis, and treatment options for rheumatoid arthritis. *Cells*. 2020;9(4):880.
5. Zheng H, Liu Y, Deng Y, et al. Recent advances of NFATc1 in rheumatoid arthritis-related bone destruction: mechanisms and potential therapeutic targets. *Mol Med*. 2024;30(1):20.
6. Xu HC, Hu K, Shi XH, et al. Synergistic use of NMR computation and quantitative interproton distance analysis in the structural determination of neokadcoccitane A, a rearranged triterpenoid featuring an aromatic ring D from *Kadsura coccinea*. *Org Chem Front*. 2019;6(10):1619–1626. doi:10.1039/C9QO00281B
7. Yang YP, Jian YQ, Liu YB, et al. Heilaohuacid G, a new triterpenoid from *Kadsura coccinea* inhibits proliferation, induces apoptosis, and ameliorates inflammation in RA-FLS and RAW 264.7 cells via suppressing NF-?B pathway. *Phytother Res*. 2022;36(10):3900–3910. doi:10.1002/ptr.7527
8. Ansalone C, Cole J, Chilaka S, et al. TNF is a homoeostatic regulator of distinct epigenetically primed human osteoclast precursors. *Ann Rheum Dis*. 2021;80(6):748–757. doi:10.1136/annrheumdis-2020-219262
9. Xu H, Zhao H, Fan D, et al. Interactions between gut microbiota and immunomodulatory cells in rheumatoid arthritis. *Mediators Inflamm*. 2020;2020:1430605. doi:10.1155/2020/1430605
10. Li J, Kuhn KA. Microbial threads in the tapestry of rheumatoid arthritis. *J Clin Invest*. 2025;135(18). doi:10.1172/JCI195374
11. Lv J, Hao P, Zhou Y, et al. Role of the intestinal flora-immunity axis in the pathogenesis of rheumatoid arthritis-mechanisms regulating short-chain fatty acids and Th17/Treg homeostasis. *Mol Biol Rep*. 2025;52(1):617. doi:10.1007/s11033-025-10714-w
12. Chasov V, Gilyazova E, Ganeeva I, et al. Gut microbiota modulation: a novel strategy for rheumatoid arthritis therapy. *Biomolecules*. 2024;14(12):1653. doi:10.3390/biom14121653
13. Dobinson HC, Anderson TP, Chambers ST, Doogue MP, Seaward L, Werno AM. Antimicrobial treatment options for granulomatous mastitis caused by *Corynebacterium* species. *J Clin Microbiol*. 2015;53(9):2895–2899. doi:10.1128/JCM.00760-15
14. Yu Z, Xiaojia L, Wei Z, et al. Baicalin circumvents anti-PD-1 resistance by regulating the gut microbiota metabolite short-chain fatty acids. *Pharmacol Res*. 2024;199:107033. doi:10.1016/j.phrs.2023.107033
15. Zhao T, Wei Y, Zhu Y, et al. Gut microbiota and rheumatoid arthritis: from pathogenesis to novel therapeutic opportunities. *Front Immunol*. 2022;13:1007165. doi:10.3389/fimmu.2022.1007165
16. Yang Y, Guo T, Huang F, et al. α-Glucosidase inhibitory flavonol glycosides from Cyclocarya paliurus (Batalin) Iljinskaja and their kinetics characteristics. *Phytochemistry*. 2024;225:114195. doi:10.1016/j.phytochem.2024.114195
17. Zheng H, Li Y, Deng Y, et al. Xuetongsu attenuates bone destruction in collagen-induced arthritis mice by inhibiting osteoclast differentiation and promoting osteoclast apoptosis. *Int J Biochem Cell Biol*. 2024;169:106550. doi:10.1016/j.biocel.2024.106550
18. Krenn V, Morawietz L, Burmester GR, et al. Synovitis score: discrimination between chronic low-grade and high-grade synovitis. *Histopathology*. 2006;49(4):358–364. doi:10.1111/j.1365-2559.2006.02508.x
19. Krenn V, Morawietz L, Häupl T, Neidel J, Petersen I, König A. Grading of chronic synovitis--a histopathological grading system for molecular and diagnostic pathology. *Pathol Res Pract*. 2002;198(5):317–325. doi:10.1078/0344-0338-5710261
20. Zhenyu Z, Lulu L, Huibo T, et al. Synovial fibroblast derived small extracellular vesicles miRNA15-29148 promotes articular chondrocyte apoptosis in rheumatoid arthritis. *Bone Res*. 2025;13(1):61.
21. Tang L, Wang Y, Zheng S, Bao M, Zhang Q, Li J. PTPN22 polymorphisms, but not R620W, were associated with the genetic susceptibility of systemic lupus erythematosus and rheumatoid arthritis in a Chinese Han population. *Hum Immunol*. 2016;77(8):692–698. doi:10.1016/j.humimm.2016.04.021
22. Peng Z, Huang W, Tang M, et al. Investigating the shared genetic architecture between hypothyroidism and rheumatoid arthritis. *Front Immunol*. 2023;14:1286491. doi:10.3389/fimmu.2023.1286491
23. Bénédicte A-N, Cristina PME, Frédéric B, et al. Lactiplantibacillus Plantarum strengthens the intestinal barrier: involvement of the endocannabinoidome. *Am J Physiol Gastrointest Liver Physiol*. 2025;329(2):G245–60.
24. Fang W, Zhaoyong Z, Qili L, et al. Papain-like protease of SARS-CoV-2 induces intestinal inflammation via the ISG15 pathway: identification of natural compound inhibitors. *J Med Virol*. 2025;97(6):e70448.

25. Qing W, Chun-Zheng L, Bai-Tian L, et al. Ozone controls the metabolism of tryptophan protecting against sepsis-induced intestinal damage by activating aryl hydrocarbon receptor. *World J Gastroenterol*. 2025;31(17):105411.
26. Agirman G, Yu KB, Hsiao EY. Signaling inflammation across the gut-brain axis. *Science*. 2021;374(6571):1087–1092. doi:10.1126/science.abi6087
27. Chen P, Luo Z, Lu C, Jian G, Qi X, Xiong H. Gut-immunity-joint axis: a new therapeutic target for gouty arthritis. *Front Pharmacol*. 2024;15:1353615. doi:10.3389/fphar.2024.1353615
28. Meng Q, Lin M, Song W, et al. The gut-joint axis mediates the TNF-induced RA process and PBMT therapeutic effects through the metabolites of gut microbiota. *Gut Microbes*. 2023;15(2):2281382. doi:10.1080/19490976.2023.2281382
29. Pan P, Wang Y, Nyirenda MH, et al. Undenatured type II collagen protects against collagen-induced arthritis by restoring gut-joint homeostasis and immunity. *Commun Biol*. 2024;7(1):804. doi:10.1038/s42003-024-06476-z
30. Hongyang L, Xiangbowen J, Binbin C, et al. Inflammation targeting and responsive multifunctional drug-delivery nanoplatforms for combined therapy of rheumatoid arthritis. *Small*. 2025;21(22):2500113.
31. Xuyang X, Chenjia H, Zhinan X, et al. Single cell immunoprofile of synovial fluid in rheumatoid arthritis with TNF/JAK inhibitor treatment. *Nat Commun*. 2025;16(1):2152.
32. Tom T, Matthias F, Charlotte R-G, et al. A longitudinal single-cell atlas of anti-tumour necrosis factor treatment in inflammatory bowel disease. *Nat Immunol*. 2024;25(11):2152–2165.
33. Alessandra N, Marie-Astrid B, Giulia Maria G, et al. Axl and MerTK regulate synovial inflammation and are modulated by IL-6 inhibition in rheumatoid arthritis. *Nat Commun*. 2024;15(1):2398.
34. Hui W, Hanmei Y, Jin Z, et al. Helicobacter pylori upregulates PAD4 expression via stabilising HIF-1α to exacerbate rheumatoid arthritis. *Ann Rheum Dis*. 2024;83(12):1666–1676.
35. Chia-Hao L, Cheng-Jang W, Sunglim C, et al. Selective IL-27 production by intestinal regulatory T cells permits gut-specific regulation of T(H)17 cell immunity. *Nat Immunol*. 2023;24(12):2108–2120.
36. Nadine B, Daniel M, Christian A, et al. Additive efficacy of a bispecific anti-TNF/IL-6 nanobody compound in translational models of rheumatoid arthritis. *Sci Transl Med*. 2023;15(681):eabq4419.
37. Guo Y, Tian M, Liu Y, et al. New bitongling ameliorates joint tissue damage in collagen-induced arthritis mice by suppressing mapt expression: a genome-wide sequencing study. *J Inflamm Res*. 2025;18:15597–15614. doi:10.2147/JIR.S557354